Ecosystem physio-phenology revealed using circular statistics
Supplementary information (I)

Daniel E. Pabon-Moreno[1], Talie Musavi[1], Mirco Migliavacca[1], Markus Reichstein[1,2], Christine Römermann[2,3], and Miguel D. Mahecha[1,2]

[1]Max Planck Institute for Biogeochemistry, Hans–Knoell–Str. 10, 07745 Jena, Germany.
[2]German Centre for Integrative Biodiversity Research (iDiv), Deutscher Platz 5e, 04103 Leipzig, Germany.
[3]Friedrich Schiller University, Institute of Ecology and Evolution, Philosophenweg 16, D-07743 Jena, Germany.

1 Half-time sensitivity analysis (System memory to explain DOY_{GPPmax})

The optimum halftime parameter is estimated for each site showing that for most of the unimodal sites JS correlation is maximum when the halftime parameter takes values between 2 and 100 days. Per vegetation type Deciduous Broadleaf Forest (DBF), Evergreen Needleleaf Forest (ENF) and Grassland (GRA) have similar values for the optimum half-time parameter (Figure S3). Per climate classes, the oceanic climate (Cfb) has the highest variation. There are only 2 unimodal sites with an optimum half-time greater than 180 days: IT-MBo and FR-Fon. On the other hand, for the bimodal site (ES-LJu) the maximum JS coefficient is obtained with a half-time of 13 for the first growing season and 21 days for the second one (Table S2). Estimating the halftime of the drivers per site is a prerequisite for optimizing the predictions with the circular regressions in the next step. For most of the sites, the JS correlation coefficient is maximum between 0.98 and 0.7 (Figure S5).

Our results for the optimum halftime parameter between 2 and 100 days for all sites are similar to the time window length of 15 to 120 days required to explain the variations on the leaf unfolding for different tree species in Europe (Fu et al., 2015). Or, the time window length of 45 to 95 days to explain the flowering day of different plant species in Switzerland (Güsewell et al., 2017). No matter what phenological event is being analyzed all studies agree that phenological events are influenced by past climatic conditions in a cumulative form.

In our case, the use of a half-life decay function changes the interpretation of the optimum halftime day parameter indicating that half of the contribution is given before the halftime day in an exponential form and that the contribution of the rest of the days is low, but not equal to 0. Finally, we find that the optimum half-time is not necessarily related to the vegetation type or the predominant climate class in each site. We suggest that it could be more related to the species dominance and the spatial arrangement and the intraspecific climatic variability of each site.

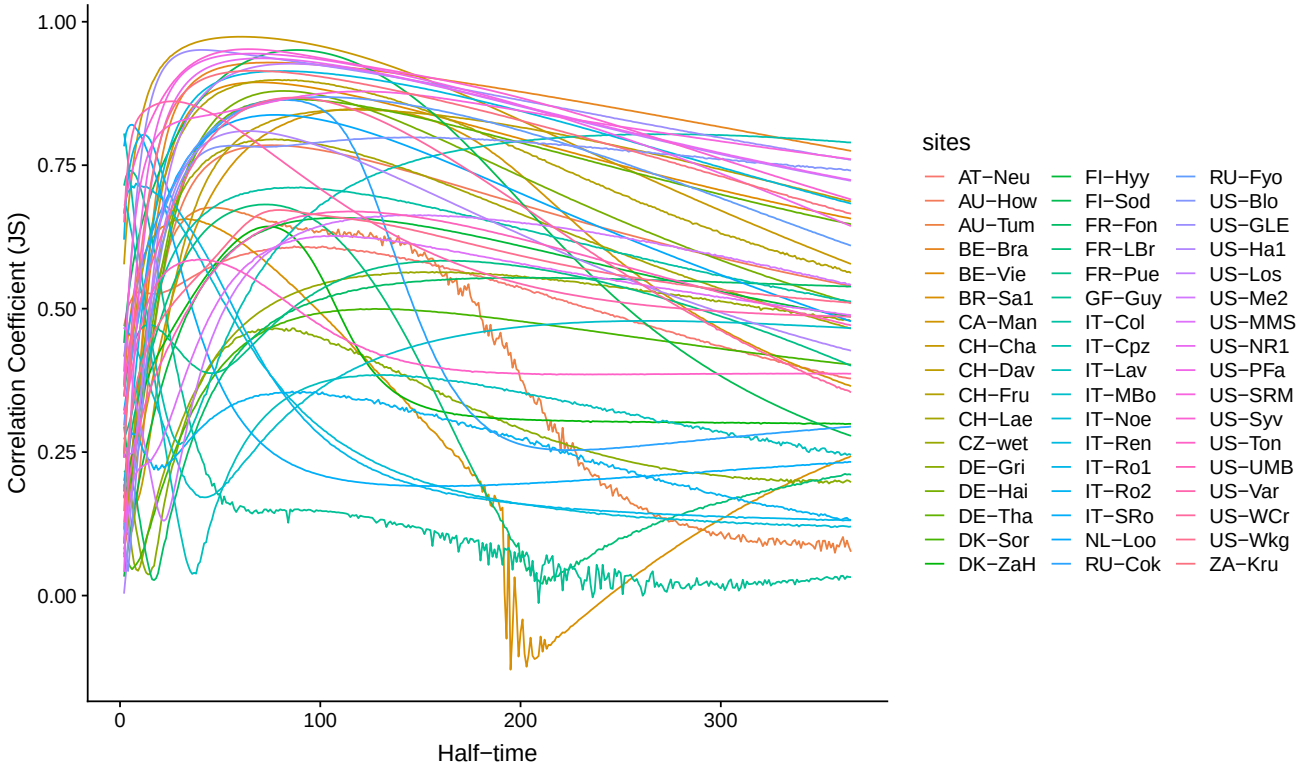

Figure S1. Half-time sensitivity analysis. The correlation coefficient (JS) between the observed and predicted DOY_{GPPmax} using different half-time values. Each FLUXNET site is represented with a color.

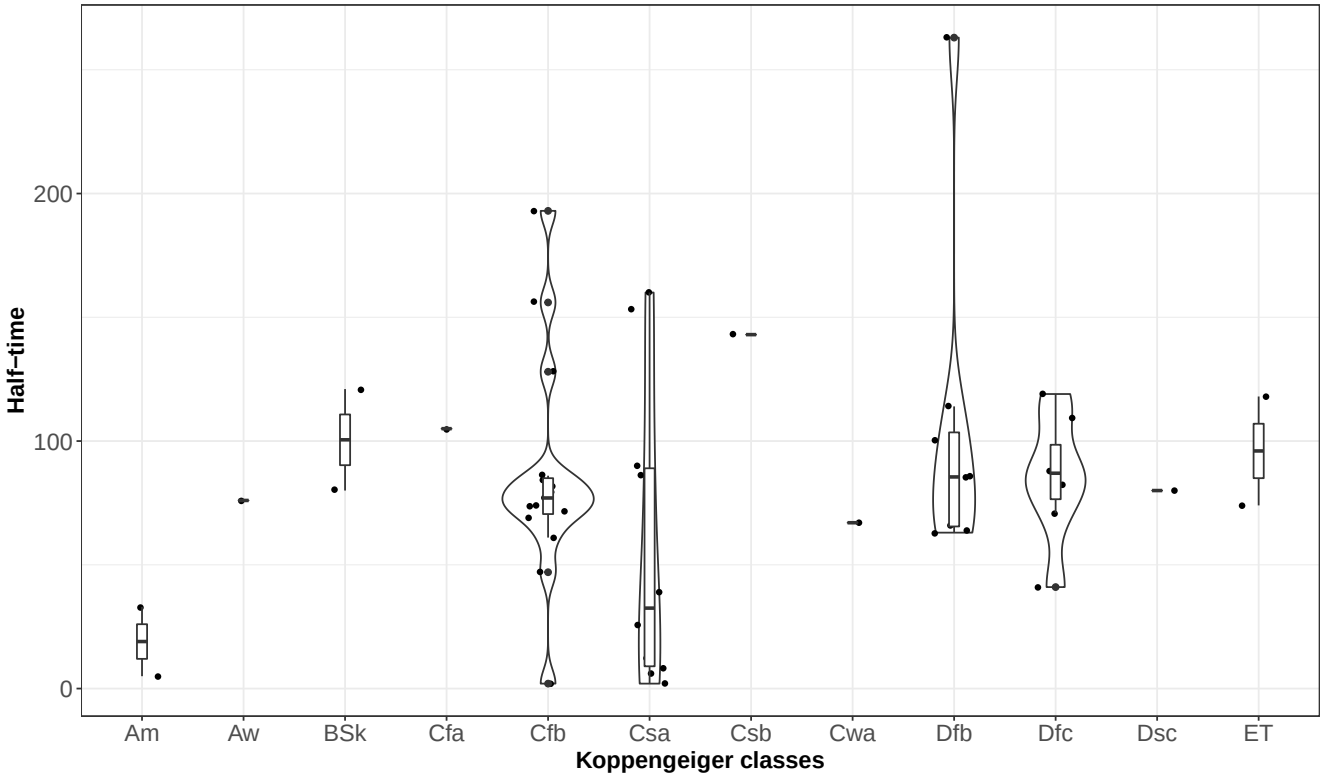

Figure S2. Half-time sensitivity analysis. Distribution of the half-time when the Jammalamanaka-Sarna (JS) coefficient is maximum for each FLUXNET site using as classification criterium the Koppen climate classes: Tropical monsoon climate (Am), Tropical savanna climate (Aw), Cold semi-arid climates (BSk), Humid subtropical climate (Cfa), Oceanic climate (Cfb), Hot-summer mediterranean climate (Csa), Warm-summer mediterranean climate (Csb), Humid subtropical climate (Cwa), humid continental climate (Dfb), Subarctic climate (Dfc, Dsc), and Tundra climate (ET)

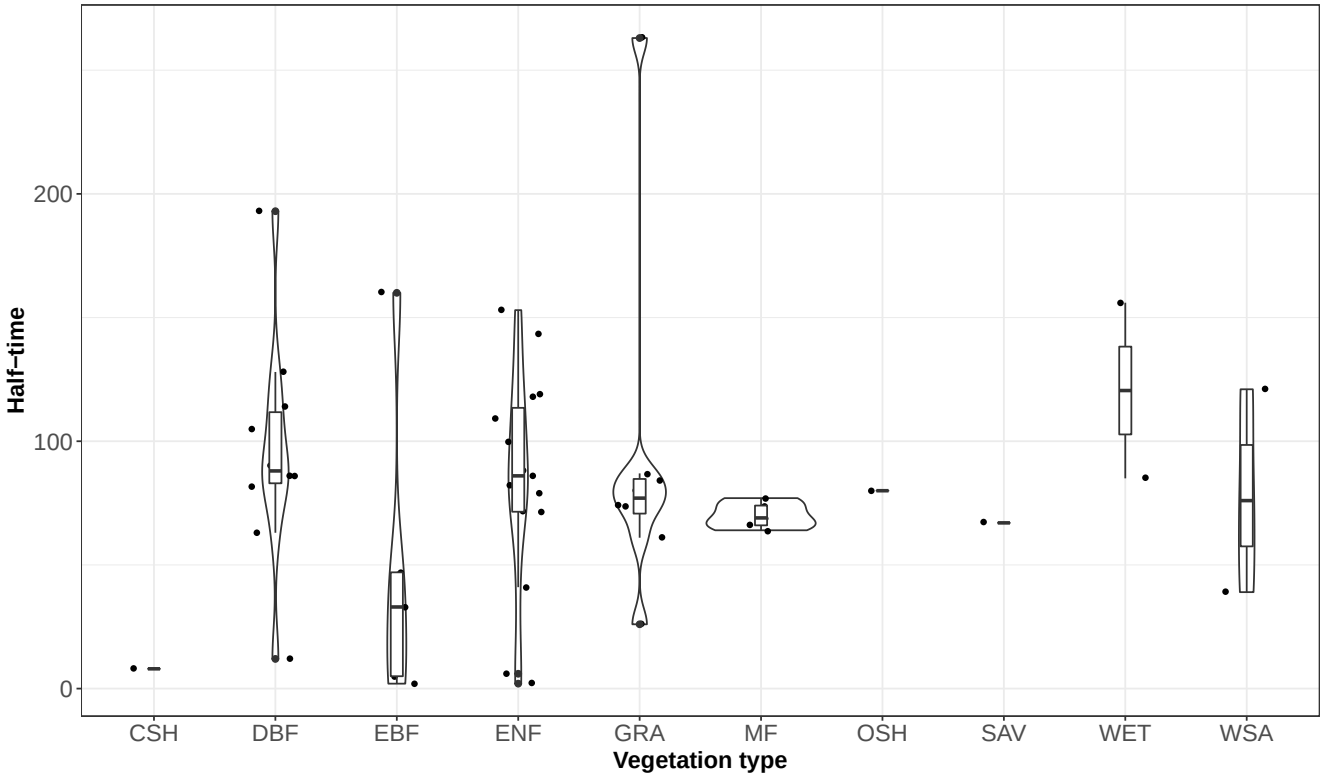

Figure S3. Half-time sensitivity analysis. Distribution of the optimum half-time parameter when the Jammalamadaka-Sarna (JS) coefficient is maximum per vegetation type. Closed Shrublands (CSH), Deciduous Broadleaf Forests (DBF), Evergreen Broadleaf Forests (EBF), Evergreen Needleleaf Forests (ENF), Grasslands (GRA), Mixed Forests (MF), Open Shrublands (SAV) Savannas, Permanent Wetlands (WET), Woody Savannas (WSA)

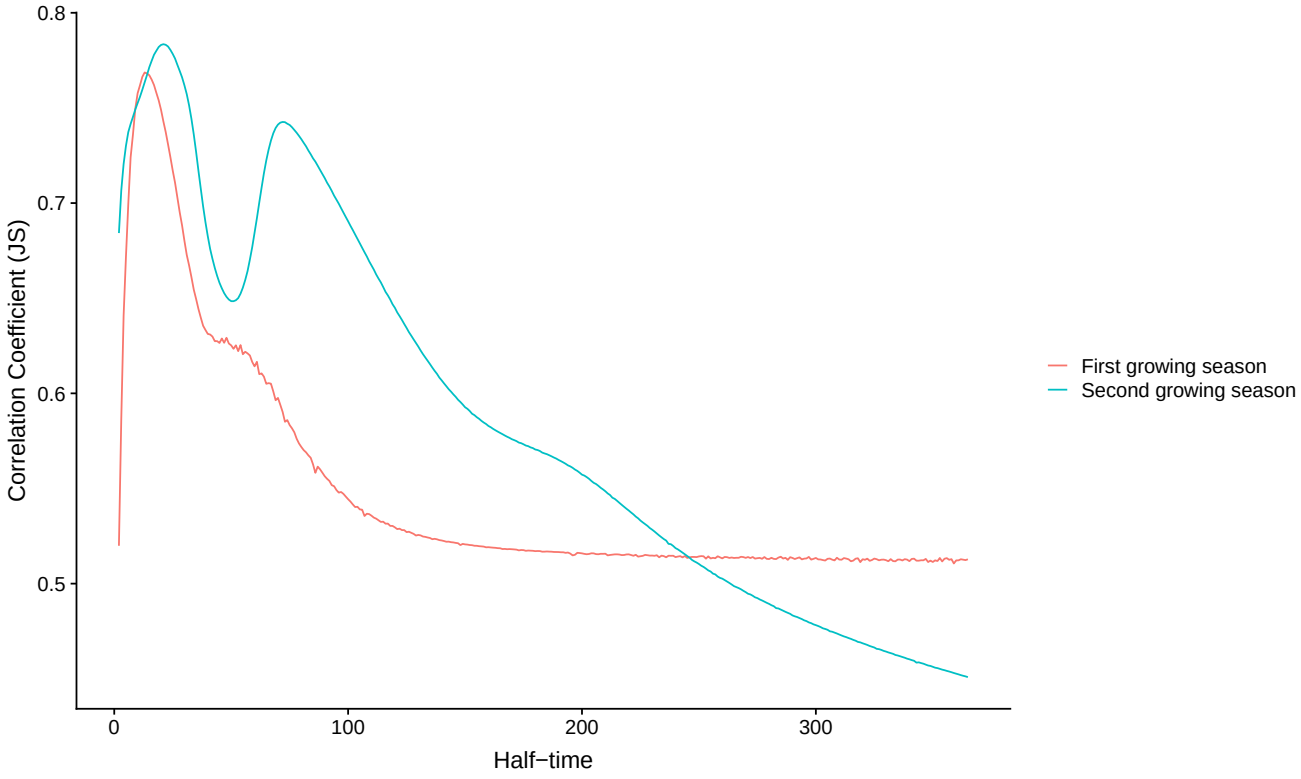

Figure S4. Half-time sensitivity analysis for ES-LJu the unique FLUXNET site analyzed with two growing seasons.

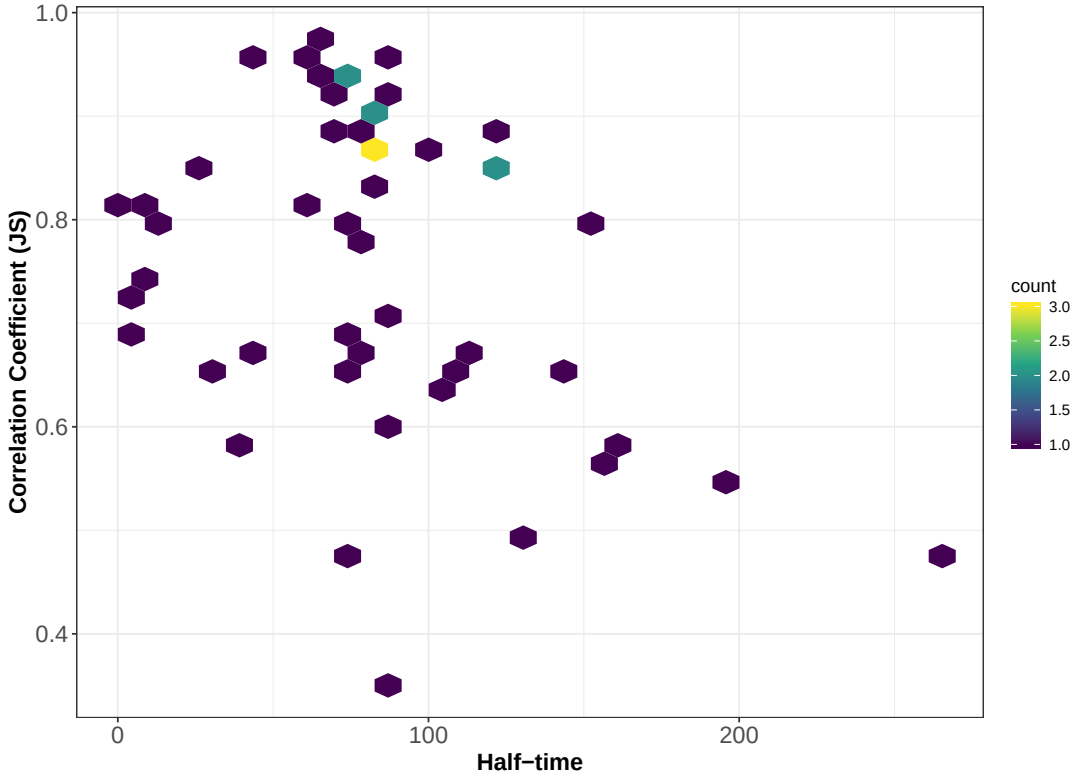

Figure S5. Distribution of the maximum correlation coefficient values when the optimum halftime has been used. Most of the sites have the maximum correlation coefficient when half-time is between 5 and 100 days.

Table S1: Optimum half-time coefficient and correlation coefficient per FLUXNET site. We report the name of sites, the climate class of the site following the Köppen-Geiger classification: Tropical monsoon climate (Am), Tropical savanna climate (Aw), Cold semi-arid climates (BSk), Humid subtropical climate (Cfa), Oceanic climate (Cfb), Hot-summer mediterranean climate (Csa), Warm-summer mediterranean climate (Csb), Humid subtropical climate (Cwa), humid continental climate (Dfb), Subarctic climate (Dfc, Dsc), and Tundra climate (ET). We also report the vegetation type where: We also report the Vegetation type: Closed Shrublands (CSH), Deciduous Broadleaf Forests (DBF), Evergreen Broadleaf Forest (EBF), Evergreen Needleleaf Forests (ENF), Grasslands (GRA), Mixed Forests (MF), Open Shrublands (OSH), Savannas (SAV), Permanent Wetlands (WET), Woody Savannas (WSA).

Site name	Köppen-Geiger class	Vegetation type	Half-time	Correlation coefficient (JS)
US-Ha1	Dfb	DBF	63	0.81
US-PFa	Dfb	MF	66	0.94
BE-Bra	Cfb	MF	74	0.93
BE-Vie	Cfb	MF	69	0.89
DE-Tha	Cfb	ENF	86	0.86
DK-Sor	Cfb	DBF	128	0.5
FI-Hyy	Dfc	ENF	109	0.66
IT-Col	Csa	DBF	90	0.71
NL-Loo	Cfb	ENF	79	0.84
CH-Dav	ET	ENF	118	0.85
RU-Fyo	Dfb	ENF	100	0.87
US-NR1	Dfc	ENF	71	0.94
IT-Ren	Dfc	ENF	82	0.91
US-MMS	Cfa	DBF	105	0.63
US-WCr	Dfb	DBF	86	0.87
CA-Man	Dfc	ENF	119	0.85
DK-ZaH	ET	GRA	74	0.64
FR-Pue	Csa	EBF	160	0.58
US-Los	Dfb	WET	85	0.93
US-UMB	Dfb	DBF	114	0.67
US-Var	Csa	GRA	26	0.86
AU-How	Aw	WSA	76	0.78
AU-Tum	Cfb	EBF	47	0.68
FI-Sod	Dfc	ENF	88	0.95

IT-SRo	Csa	ENF	6	0.82
US-Syv	Dfb	MF	64	0.95
US-Ton	Csa	WSA	39	0.59
ZA-Kru	Cwa	SAV	67	0.91
DE-Hai	Cfb	DBF	82	0.88
FR-LBr	Cfb	ENF	72	0.68
IT-Cpz	Csa	EBF	2	0.81
US-Me2	Csb	ENF	143	0.66
IT-Lav	Cfb	ENF	2	0.68
RU-Cok	Dsc	OSH	80	0.86
AT-Neu	Dfc	GRA	87	0.61
CH-Lae	Cfb	MF	77	0.8
DE-Gri	Cfb	GRA	74	0.47
GF-Guy	Am	EBF	5	0.74
IT-MBo	Dfb	GRA	263	0.48
IT-Noe	Csa	CSH	8	0.72
IT-Ro2	Csa	DBF	86	0.36
US-Blo	Csa	ENF	153	0.8
US-GLE	Dfc	ENF	41	0.95
US-SRM	BSk	WSA	121	0.88
US-Wkg	BSk	GRA	80	0.67
BR-Sa1	Am	EBF	33	0.66
CH-Cha	Cfb	GRA	61	0.97
CH-Fru	Cfb	GRA	84	0.9
FR-Fon	Cfb	DBF	193	0.55
CZ-wet	Cfb	WET	156	0.56
IT-Ro1	Csa	DBF	12	0.8

Table S2. Results of the optimum half-time and the maximum correlation coefficient for " Llano de los Juanes", Spain with Köppen-Geiger class: Hot-summer Mediterranean climate (Csa) and vegetation type: Open Shrublands (OSH)

			DOY_{GPPmax} (GS 1)		DOY_{GPPmax} (GS 2)	
Site name	Köppen-Geiger class	Vegetation type	Optimum Halftime	Correlation coefficient (JS)	Optimum Halftime	Correlation coefficient (JS)
ES-Lju	Csa	OSH	13	0.77	21	0.78

2 Phenological summary of the FLUXNET sites (Recovering DOY_{GPPmax})

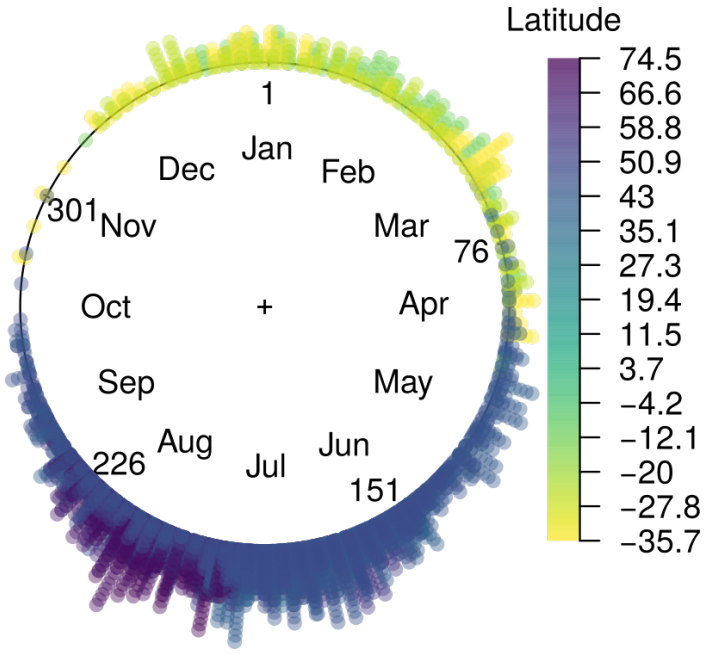

Figure S6. DOY_{GPPmax} distribution across the latitudinal gradient. Most of the DOY_{GPPmax} is reached at the middle of the year. This pattern is generated by the geographical trend of the location of the FLUXNET network in the Northern hemisphere.

Table S3: Mean angular direction and the standard deviation of DOY_{GPPmax} for ecosystems with one growing season per year.

Site name	Mean DOY_{GPPmax} (days)	SD DOY_{GPPmax} (days)
US-Ha1	195.2	19.5
US-PFa	196.6	21.6
BE-Bra	196.71	25.35
BE-Vie	192.28	29.9
DE-Tha	182.91	27.4
DK-Sor	169.96	13.96
FI-Hyy	199.93	17.74
IT-Col	187.75	23.84
NL-Loo	210.27	25.82
CH-Dav	180.99	38.69
RU-Fyo	192.14	23.17

US-NR1	201.98	28.79
IT-Ren	193.55	32.34
US-MMS	183.59	22.71
US-WCr	198.26	20.02
CA-Man	215.87	19.96
DK-ZaH	204.39	10.3
FR-Pue	159.97	34.07
US-Los	194.81	13.46
US-UMB	189.13	20.5
US-Var	95.95	21.82
AU-How	28.77	30.87
AU-Tum	24.29	46.9
FI-Sod	214.35	15.66
IT-SRo	142.6	28.3
US-Syv	194.9	25.65
US-Ton	114.63	20
ZA-Kru	15.35	37.09
DE-Hai	190.26	22.84
FR-LBr	177.35	23.83
IT-Cpz	154.5	46.04
US-Me2	182.5	26.15
IT-Lav	167.19	37.11
RU-Cok	209.61	11.48
AT-Neu	161.46	33.73
CH-Lae	185.32	30.71
DE-Gri	178.61	33.51
GF-Guy	214.86	41.17
IT-MBo	169.51	12.22
IT-Noe	120.71	28.96
IT-Ro2	155.48	18.69
US-Blo	199.04	33.38
US-GLE	209.55	17.46
US-SRM	227.65	17.66

US-Wkg	228.54	11.26
BR-Sa1	325.24	38.49
CH-Cha	201.24	38.2
CH-Fru	163.9	39.97
FR-Fon	179.49	24.11
CZ-wet	169.88	17.68
IT-Ro1	148.23	11.33

Table S4. Mean angular direction and standard deviation of DOY_{GPPmax} for ecosystems with two growing seasons

			DOY_{GPPmax} (GS 1)		DOY_{GPPmax} (GS 2)	
Site name	Koppen	Vegetation type	Mean (DOY)	SD (days)	Mean (DOY)	SD (days)
ES-Lju	Csa	OSH	143.62	17.84	302.63	19.18

3 Similarity of regression coefficients per vegetation type and climate classes

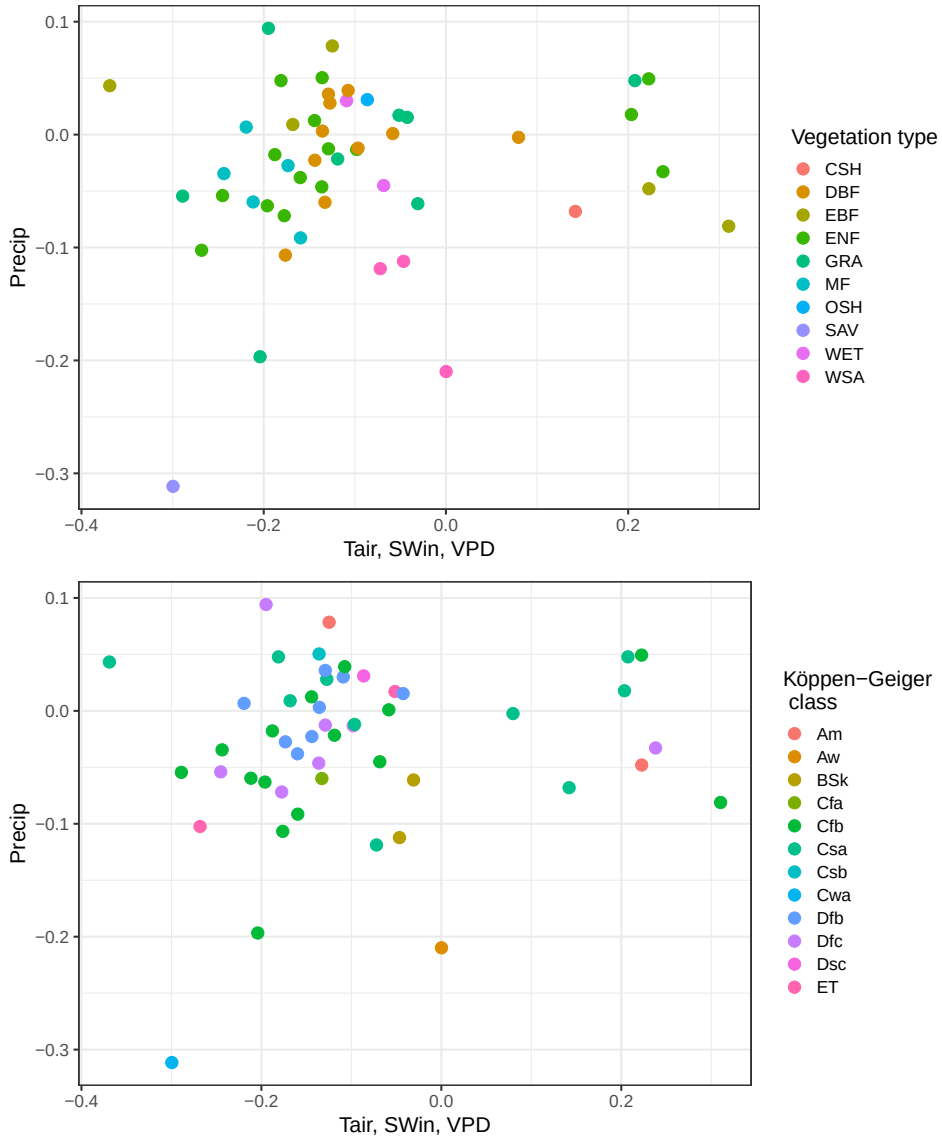

Figure S7. Regression coefficient values of the first component of the PCA of air temperature, shortwave incoming radiation, and vapor pressure deficit, and precipitation. a). Colors per the vegetation: Closed Shrublands (CSH), Deciduous Broadleaf Forests (DBF), Evergreen Broadleaf Forest (EBF), Evergreen Needleleaf Forests (ENF), Grasslands (GRA), Mixed Forests (MF), Open Shrublands (OSH), Savannas (SAV), Permanent Wetlands (WET), Woody Savannas (WSA). c) Colors per Köppen-Geiger climate classes: Tropical monsoon climate (Am), Tropical savanna climate (Aw), Cold semi-arid climates (BSk), Humid subtropical climate (Cfa), Oceanic climate (Cfb), Hot-summer mediterranean climate (Csa), Warm-summer mediterranean climate (Csb), Humid subtropical climate (Cwa), humid continental climate (Dfb), Subarctic climate (Dfc, Dsc), and Tundra climate (ET)

References

Fu, Y. H., Zhao, H., Piao, S., Peaucelle, M., Peng, S., Zhou, G., Ciais, P., Huang, M., Menzel, A., Peñuelas, J., Song, Y., Vitasse, Y., Zeng, Z., and Janssens, I. A.: Declining global warming effects on the phenology of spring leaf unfolding, Nature, 526, 104–107, https://doi.org/10.1038/nature15402, https://www.nature.com/articles/nature15402, 2015.

Güsewell, S., Furrer, R., Gehrig, R., and Pietragalla, B.: Changes in temperature sensitivity of spring phenology with recent climate warming in Switzerland are related to shifts of the preseason, Global Change Biology, 23, 5189–5202, https://doi.org/10.1111/gcb.13781, http://onlinelibrary.wiley.com/doi/10.1111/gcb.13781/abstracthttp://onlinelibrary.wiley.com/store/10.1111/gcb.13781/asset/gcb13781.pdf?v=1&t=jdmyu5yf&s=8101659af8b310121d3227eb531cf4166cbfc8a8, 2017.